Contents lists available at ScienceDirect

Transactions of Nonferrous Metals Society of China

36(2026) 231−243

www.tnmsc.cn

Distinctive yield behavior of low-density Co−Ni−Al−V−Ti−Ta superalloy designed by CALPHAD

Yu-peng ZHANG [a,b], Zhong-feng CHEN [a,b], De-bin ZHENG [a,b], Cui-ping WANG [a,b,*], Hao-jun ZHUO [a,b], Xiang YU [a,b], Yue-chao CHEN [a,b], Shui-yuan YANG [a,b,**], Yi-lu ZHAO [c], Xing-jun LIU [c,***]

[a] Fujian Key Laboratory of Surface and Interface Engineering for High Performance Materials, School of Materials Science, Xiamen University, Xiamen 361005, China;

[b] Xiamen Key Laboratory of High Performance Metals and Materials, School of Materials Science, Xiamen University, Xiamen 361005, China;

[c] School of Materials Science and Engineering, Harbin Institute of Technology (Shenzhen), Shenzhen 518055, China

Abstract: Low-density superalloys often exhibit low yield strength in the intermediate temperature range (300−650 °C). To enhance yield performance in this range, the CALPHAD method was used to design a new Co-based superalloy. The Co−30Ni−10Al−3V−6Ti−2Ta alloy, designed based on γ' phase dissolution temperature and phase fraction, was synthesized via arc melting and heat treatment. Phase transition temperatures, microstructure evolution, and high-temperature mechanical properties were characterized by differential scanning calorimetry, scanning electron microscopy, dual-beam TEM, and compression tests. Results show that the alloy has low density (8.15 g/cm³) and high γ' dissolution temperature (1234 °C), along with unique yield strength retention from room temperature to 650 °C. The yield strength anomaly (YSA) is attributed to high stacking fault energy and activation of the Kear−Wilsdorf locking mechanism, contributing to superior high-temperature stability of the alloy. The yield strength of this alloy outperforms other low-density Co-based superalloys in the temperature range of 23−650 °C.

Keywords: Co-based superalloy; calculated phase diagram; mechanical property; sub microstructure evolution; γ' phase

1 Introduction

Superalloy is a key material for aerospace engine blades and hot end parts of gas engines [1−3]. Among many types of superalloys, Ni-based superalloy with the unique γ'-Ni_3Al phase strengthening mechanism is currently the most widely used commercial application material [4−7]. However, the working temperature of Ni-based superalloy is so close to its melting point that it is hard to further improve the temperature-bearing capacity [1,8−10]. Therefore, research is focused towards finding alternative superalloy materials for next generation aero-engines. In 2006, SATO et al [11] discovered a new Co−Al−W based superalloy that is strengthened by $L1_2$-γ' $Co_3(Al,W)$ phase. The melting point of this superalloy is higher than that of some Ni-based superalloys. Moreover, due to the difference between γ' dissolution temperature and γ dissolution temperature, a larger processing window was found in the Co-based superalloy [12], which is crucial to improving mechanical properties at high temperatures. Because of the above reasons, the Co-based superalloy has become a key topic of research. It has been reported that the addition of

Corresponding author: *Cui-ping WANG, E-mail: wangcp@xmu.edu.cn; **Shui-yuan YANG, E-mail: yangshuiyuan@xmu.edu.cn; ***Xing-jun LIU, E-mail: lxj@hit.edu.cn

https://doi.org/10.1016/S1003-6326(25)66960-3

Received 22 April 2024; accepted 21 February 2025

5−12 at.% W can form a stable γ'-$Co_3(Al,W)$ to maintain stable high-temperature performance in the Co−Al−W based superalloy [13−15]. However, excessive W will cause increase in the density of the superalloy. Therefore, drawbacks such as narrow γ/γ' phase region [11,16], poor high-temperature stability of $L1_2$-γ' $Co_3(Al,W)$ phase [17,18], high density [14] make the development of W-free Co-based superalloy the focus for further research.

In order to optimize superalloy density and further improve γ' phase stability, new systems like Co−Ti based [19,20], Co−Al−Mo based [21,22], Co−Al−Ta based [23,24], and Co−Al−V based [25] superalloys have been studied. Among them, Co−Ti based superalloy has lower density, but is usually accompanied by poor γ' phase stability and low mechanical properties at medium and high temperatures. As for the Co−Al−Mo superalloy, its density is comparable to that of Co−8Al−12W−14Cr superalloy (8.4 g/cm^3, at 620 MPa and 800 °C) [26], but its yield stress (620 MPa at 770 °C) is not significantly improved [27]. Moreover, both low-density Co−Ti based [19,28] and Co−Al−Mo based [29] superalloys have the disadvantage of drastic decrease in yield stress with increase in temperature, in the moderate temperature range. This is caused by the lack of high melting point alloying elements (W, Ta, etc.) in low-density superalloy, resulting in insignificant solid solution strengthening effects. Therefore, it is important to overcome the disadvantages of low-density superalloy by improving the stability and strengthening effect of γ' phase.

However, the main research method of superalloy is the trial-and-error method based on experiments, which is inefficient. For effective materials design, computational methods (density functional theory (DFT), CALPHAD, and machine learning, etc.) are used. Usually, design of new Co-based superalloy often contains multiple strengthening elements. While DFT method is time consuming [30−34], machine learning is limited by reported experimental data, and it is difficult to guarantee the accuracy of its prediction performance [35−38]. Although the CALPHAD method also relies on experimental data, the accuracy of prediction can be achieved after completing the determination of various phase regions through a relatively small amount of experimental data. Therefore, this study relies on the established experimental data [23,25,39−41], in conjunction with multivariate database developed by our research team, to utilize the CALPHAD method for accurate prediction of phase diagram of the six-element alloy. This approach forms a basis for alloy design and microstructure control.

This study aims to enhance the yield strength of low-density Co-based superalloys at intermediate temperatures. Using the CALPHAD method, we designed and synthesized the Co−30Ni−10Al−3V−6Ti−2Ta alloy, which features both low density and high γ' dissolution temperature. The alloy exhibits an abnormal yield behavior starting from room temperature, effectively addressing the low yield strength issue of Co-based alloys at intermediate temperatures. This work provides both experimental data and theoretical guidance for the design of lightweight superalloys.

2 Experimental

In this study, design of Co−Ni−Al−V−Ti−Ta superalloy was conducted using the CALPHAD method implemented in the Pandat software, leveraging the Co-based superalloy database developed by our research group [23,25,39,40]. Further details of the design process are provided below.

Ingots weighing approximately 60 g, were produced in an arc-melting furnace under an argon atmosphere using high-purity Co (99.9 wt.%), Ni (99.9 wt.%), V (99.9 wt.%), Al (99.9 wt.%), Ti (99.9 wt.%), and Ta (99.9 wt.%). The composition of superalloy (Co−30Ni−10Al−3V−6Ti−2Ta) is typically expressed in atomic percentages unless stated otherwise. After being wire-cut into specific shapes, the samples were placed in quartz capsules filled with argon and subjected to heat treatment, first at 1250 °C for 24 h, next at 800 °C for 150 h, and were finally quenched in ice water. The phase transition temperature of the superalloy was measured using a differential scanning calorimetry (DSC, NETZSCH, Germany), in a high-purity argon atmosphere with a heating rate of 20 °C/min. Microstructure of polished specimens (etched in a solution of 25% HNO_3 and 75% HCl), was observed using a field emission scanning electron microscope (SEM, Su70, Japan). TEM samples were polished by twin-jet polishing in 8% $HClO_4$ + 92% C_2H_6O. To determine the crystal structure of phases, a

transmission electron microscope (TEM, Tecnai−F30, FEI) was utilized. Chemical compositions of γ/γ' phases were analyzed using STEM−EDX techniques. Additionally, the 0.2% deformation structure observed in the TEM experiments refers to the microstructure obtained after the alloy is loaded to its yield stress at the corresponding temperature, followed by slow unloading and rapid cooling. The density of the newly developed superalloy was determined according to ASTM B311 — 08 recommendations, which utilized Archimedes principle. Vickers hardness measurement was carried out using Vickers micro hardness tester (HMV−2, Japan), at an applied load of 4.9N. For compression testing, samples with dimensions of d4 mm × 6 mm were obtained by wire cutting. Compression tests were performed at various temperatures ranging from room temperature to 900 °C using a universal testing machine (WDW−100, China). The strain rate was set at 1×10^{-4} s^{-1}. At least three samples were tested for each temperature investigated.

3 Superalloy design and validation

3.1 Design and validation of Co−Ni−Al−V−Ti−Ta superalloy

The stable γ' phase is the key to maintaining good high-temperature properties. In addition to the stable Co_3Ti phase [42], $Co_3(Al,V)$ phase has also been proven to be a thermodynamically stable phase in novel Co-based superalloy [25]. The addition of V facilitates the formation of γ'-$Co_3(Al,V)$ phase within the alloy system, which can enhance the stability of the alloy's performance at high temperatures [25]. However, higher V content compromises the oxidation resistance and coarsening rate of superalloys [43]. Therefore, the determination of V content is a challenging problem. Figure 1(a) illustrates the pseudo-binary phase diagram of the Co−30Ni−10Al−xV system, indicating a significant γ/γ' two-phase region between 800 and 1000 °C. As V content increases, the γ' dissolution temperature gradually rises, and the solidus temperature (γ dissolution temperature) decreases. It is noteworthy that the increase rate in γ' dissolution temperature slows down as the V content increases. Therefore, considering the magnitude and growth rate of γ' dissolution temperature, this study selects 3 at.% V as the focus for further investigation. However, the phase fraction of Co−30Ni−10Al−3V alloy at 800 °C is only 23% (Fig. 1(d)), which is also the reason for further alloying.

Figure 1(b) depicts the pseudo-binary phase diagram following Ti alloying. The γ' dissolution temperature increases with Ti addition. However, the

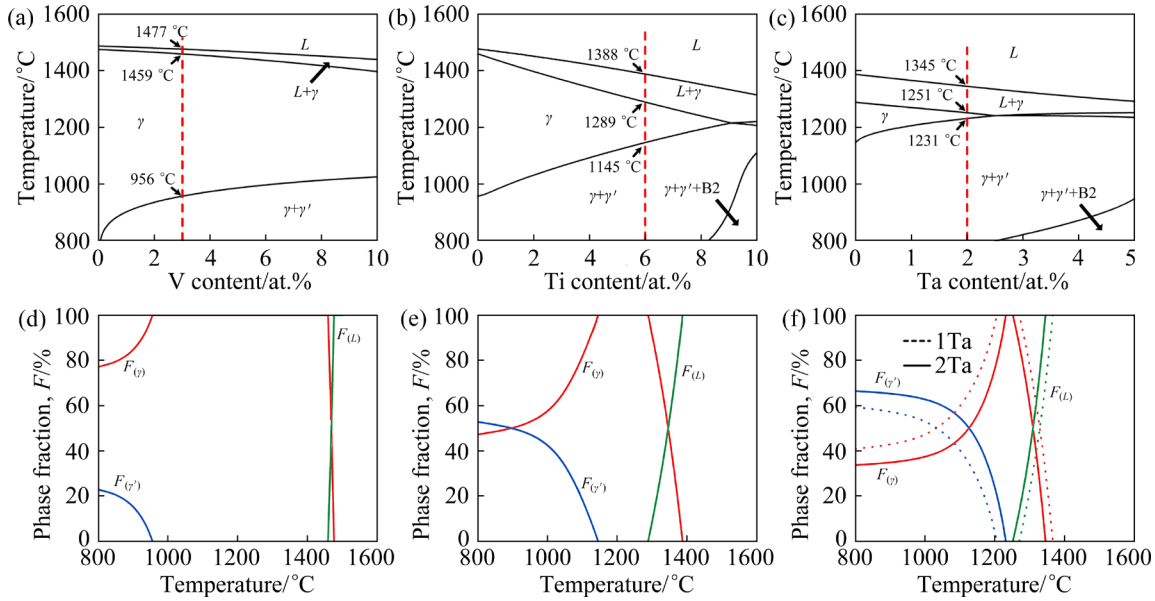

Fig. 1 Calculated pseudo-binary phase diagrams of (a) Co−30Ni−10Al−xV, (b) Co−30Ni−10Al−3V−xTi, and (c) Co−30Ni−10Al−3V−6Ti−xTa systems; Calculated fractions of each phase versus temperature of (d) Co−30Ni−10Al−3V, (e) Co−30Ni−10Al−3V−6Ti, (f) Co−30Ni−10Al−3V−6Ti−1Ta (dashed line) and Co−30Ni−10Al−3V−6Ti−2Ta (solid line)

difference (thermal processing window) between the solidus and γ' dissolution temperature gradually decreases. The Co−30Ni−10Al−3V−6Ti alloy exhibits a thermal processing window of 144 °C, ranging from 1145 to 1289 °C. Meanwhile, the thermal processing window of Co−30Ni−10Al−3V−7Ti alloy is 94 °C, ranging from 1171 to 1265 °C. A larger thermal processing window facilitates alloying of other γ'-forming elements. Considering the beneficial effects of Ta, which significantly enhances the alloy's complex stacking fault (CSF) energy and the anti-phase boundary energy on the (111) plane, thereby improving the alloy's strength and high-temperature performance stability [44], a wider thermal processing window (6 at.% Ti) was selected as the focus for further alloying research. Concurrently, the phase fraction of Co−30Ni−10Al−3V−6Ti alloy also escalates from 23% to 53% at 800 °C (as indicated in Fig. 1(e)). In superalloy, maintaining γ' volume fraction exceeding 60% is crucial for ensuring favorable creep performance [1]. Consequently, Ta alloying is necessary to elevate both γ' dissolution temperature and phase fraction.

Figure 1(c) illustrates the pseudo-binary phase diagram for the Co−30Ni−10Al−3V−6Ti−xTa system. The incorporation of Ta not only raises the γ' dissolution temperature but also expands the γ'+γ two-phase region. Importantly, at Ta content of 2 at.%, the alloy exhibits a notably higher γ' dissolution temperature while still maintaining a certain thermal processing window. In Fig. 1(f), the phase fraction of Co−30Ni−10Al−3V−6Ti−xTa system is depicted. With the addition of 2 at.% Ta, in comparison to 1 at.% Ta, the phase fraction increases from 59% to 66%, and the γ' dissolution temperature rises from 1206 to 1231 °C. Consequently, this study selected the Co−30Ni−10Al−3V−6Ti−2Ta superalloy for further experimental validation.

Figure 2 illustrates the microstructure and element segregation of Co−30Ni−10Al−3V−6Ti−2Ta superalloy. White dashed lines in Fig. 2(a) represent typical grain boundaries. There are no precipitates observed at the grain boundaries. Figures 2(b, c) demonstrate TEM HAADF images of γ/γ' phases along [001] zone axis. The γ' phase fraction in 10 different regions was measured using ImageJ software, yielding an average value of 81.6%. This result is higher than the calculated value (66%) because the γ' phase approaches equilibrium at higher temperatures and longer aging time, which manifests as an increase in γ' phase size and a decrease in volume fraction [45,46]. The presence of coherent diffraction spots (Fig. 2(d)) embedded in the FCC-[001] confirms $L1_2$-ordered structure of Co−30Ni−10Al−3V−6Ti−2Ta superalloy. It can be observed that the γ' phase occupies a higher area fraction, while the γ phase appears as the black matrix phase that separates the γ' phase in high-angle annular dark-field (HAADF) image. Elemental mapping results indicate that Co is enriched in the γ phase, while Al, Ti, and Ta are primarily enriched in the γ' phase, acting as strengthening elements.

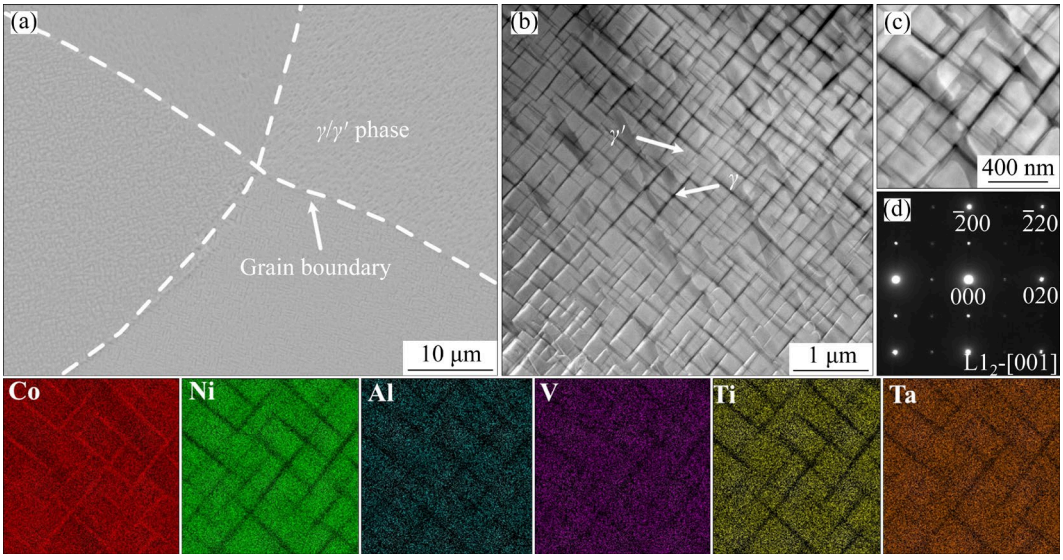

Fig. 2 (a) SEM image along grain boundary, (b, c) TEM HAADF images and (d) SAED pattern along [001] zone axis with elemental segregation images for Co−30Ni−10Al−3V−6Ti−2Ta superalloy

3.2 Comparison and analysis of superalloy performance

3.2.1 Density and γ' dissolution temperature

The DSC heating curves of Co−30Ni−10Al−3V−6Ti−2Ta superalloy as shown in Fig. 3(a). The γ' dissolution temperature and γ dissolution temperature are 1234 and 1280 °C, respectively. Importantly, the γ' dissolution temperature (1234 °C) of Co−30Ni−10Al−3V−6Ti−2Ta aligns closely with the results (1231 °C) from CALPHAD, providing further evidence of accuracy of the Co−Ni−Al−V−Ti−Ta thermodynamic database. Figure 3(b) shows the comparison of γ' dissolution temperature and density of Co−30Ni−10Al−3V−6Ti−2Ta with other Co−Ni based and Ni based superalloy. Compared to Co−Ni−Al−W based superalloy, the developed Co−30Ni−10Al−3V−6Ti−2Ta exhibits lower density and higher γ' dissolution temperature. Although the W-free Co−Ni−Al−Mo based [48], and Co−V−Ta based [36] superalloys are mainly developed for achieving low density, the low γ' dissolution temperature is a serious drawback in these systems. The γ' dissolution temperature of Co−30Ni−10Al−3V−6Ti−2Ta is significantly higher than that of Co−Ni−Al−Mo based [29,47], Co−V−Ta based [36,49], and Co−Ti based [19,40,50,51] superalloys. Furthermore, its density (8.15 g/cm^3) is also superior than that of Ni-based superalloy and the Co−Ni−Al−V based superalloy reported in our previous study [25]. This suggests that the optimized superalloy developed in this study, i.e. Co−30Ni−10Al−3V−6Ti−2Ta, shows excellent comprehensive properties of low density and high γ' dissolution temperature.

3.2.2 High-temperature yield stress

High γ' dissolution temperature is beneficial for the superalloy to maintain good mechanical properties [44,52]. However, it is difficult for low-density superalloy to have high γ' dissolution temperature and high-temperature yield stress at the same time, as observed in previous studies [19,20,29]. Low mechanical properties are often the major drawback of low-density superalloy. The mechanical property of Co−30Ni−10Al−3V−6Ti−2Ta superalloy with temperature is shown in Fig. 4. The yield stress values of Co−30Ni−10Al−3V−6Ti−2Ta superalloy are 533 MPa (room temperature), 559 MPa (150 °C), 616.3 MPa (300 °C), 607 MPa (500 °C), 610.7 MPa (650 °C), 598 MPa (700 °C),

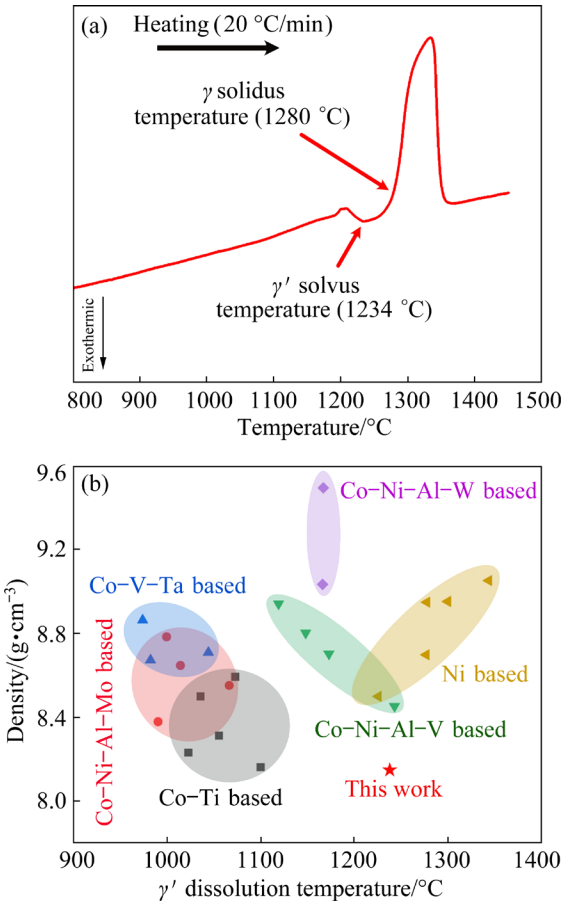

Fig. 3 (a) DSC heating curves of Co−30Ni−10Al−3V−6Ti−2Ta superalloy, and (b) comparison of γ' dissolution temperature and density of Co−30Ni−10Al−3V−6Ti−2Ta superalloy with existing superalloy, i.e. Ni based [8], Co−Ni−Al−Mo based [21,22], Co−V−Ta based [36], Co−Ti based [19,20], Co−Ni−Al−W based [26,47], and Co−Ni−Al−V based [25] superalloys

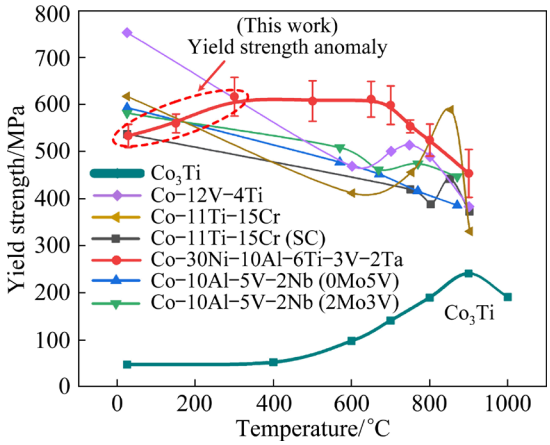

Fig. 4 Yield stress vs temperature curve of Co−30Ni−10Al−3V−6Ti−2Ta superalloy after homogenizing at 1250 °C for 24 h and aged at 800 °C for 150 h (For comparison, yield stress vs temperature responses of low density (≤8.23 g/cm^3) superalloy, Co−11Ti−15Cr (SC: single crystalline) [19,28], Co−10Al−5V−2Nb [29], and Co−12V−4Ti [20] are included)

553.3 MPa (750 °C), 524 MPa (800 °C), and 453.3 MPa (900 °C), respectively. It is noteworthy that the yield stress exhibits a gradual increase from room temperature up to 300 °C, and maintains relative stability from 300 to 650 °C (moderate temperature range). Thus, the yield strength anomaly (YSA) onset temperature is room temperature in this study, which is different from traditional low-density Co based superalloys that have a very short abnormal yield temperature range [19,20,28,29]. Although it shares the same trend as the Co_3Ti alloy, the YSA-onset temperature of this alloy is significantly lower than that of Co_3Ti alloy, which is beneficial to improving the high temperature performance stability of the alloy.

In order to provide further comparisons, Co based superalloy with low density (≤8.23 g/cm^3) reported in literature is listed, such as Co−11Ti−15Cr [19,28], Co−10Al−5V−2Nb (2Mo3V) [29] and Co−12V−4Ti [20]. As shown in Fig. 4, the yield stress at high temperature of the developed Co−30Ni−10Al−3V−6Ti−2Ta superalloy is high. Combined with low density, yield stress of Co−30Ni−10Al−3V−6Ti−2Ta superalloy is increased by 40.1% compared to the single-crystal Co−Ti−Cr superalloy [19] at 800 °C. When compared to Co−12V−4Ti superalloy, Co−30Ni−10Al−3V−6Ti−2Ta superalloy exhibits an increase in yield stress ranging from 11.1% to 30.3% between 600 and 800 °C. Also, a yield stress increases of 14.6%−32.3% can be observed when compared with Co−10Al−3V−2Nb−2Mo superalloy. The research indicates that the γ' dissolution temperature is one of the factors that determine the level of abnormal yield strength [44]. The Co−30Ni−10Al−3V−6Ti−2Ta superalloy designed in this study exhibits γ' dissolution temperatures higher than those reported for Co−Ti based superalloy (as shown in Fig. 3(b)). This also accounts for the observed phenomenon of higher strength during the exceptional yield stage of this designed alloy, surpassing the reported yield stress of other alloys.

3.3 Distinctive yield behavior

The distinctive yield phenomenon observed in the Co−30Ni−10Al−3V−6Ti−2Ta superalloy, where the YSA-onset temperature is room temperature, is not commonly seen in traditional low-density superalloys from previous studies. Given the intriguing nature of this occurrence, it has become imperative to delve into research concerning the evolution of the γ' phase substructure.

Figures 5(a, b) show STEM HAADF images along [001] zone axis for undeformed Co−30Ni−10Al−3V−6Ti−2Ta superalloy. No traces of dislocation shearing are found in γ/γ' phase. The γ' phase exhibits a typical square shape. Figures 5(c, d) show STEM HAADF images along [001] zone axis for the Co−30Ni−10Al−3V−6Ti−2Ta superalloy deformed to ~0.2% at room temperature. It is indicated that at room temperature, the deformation mechanism of the superalloy primarily entails dislocation shearing of the γ' phase. It is noteworthy that the morphological characteristics of these dislocations resemble those of primary dislocations, as opposed to the morphology of partial dislocation resulting from the dissociation of extended dislocations.

Figures 6(a, b) show TEM brightfield images taken along [011] zone axis using superlattice 200 reflection for the Co−30Ni−10Al−3V−6Ti−2Ta superalloy deformed to ~0.2% at 300 °C. It is indicated that at 300 °C, the deformation mechanism still involves dislocation shearing of γ' phase. It is noteworthy that there are distinct morphological differences between the dislocation shearing observed at 300 °C and room temperature. Figure 6(c) additionally presents a TEM weak beam dark field image capturing the dislocation slip band. Notably, the characteristics of an individual dislocation align with the reported features of a superlattice dislocation pair dissociated by an extended dislocation [53,54]. The term assigned to this singular dislocation is a superlattice dislocation pair (SDP).

Figures 6(e, f) depict TEM brightfield images taken along another [011] zone axis utilizing the superlattice [200], $[11\bar{1}]$, and $[\bar{1}1\bar{1}]$ reflection for the Co−30Ni−10Al−3V−6Ti−2Ta superalloy deformed to ~0.2% at 300 °C. Taking the six groups of superlattice dislocation pairs within the white dotted line as an example, when the diffraction reflections are $\boldsymbol{g}$=[200], $\boldsymbol{g}$=$[11\bar{1}]$, and $\boldsymbol{g}$=$[\bar{1}1\bar{1}]$, the dislocations are visible, visible, and invisible, respectively. Based on $\boldsymbol{g}\cdot\boldsymbol{b}$=0, it can be inferred that the primary dissociation of the extended dislocation mainly dissociates into $a/2$[110] partial dislocation at 300 °C. Hence, the distinction in the deformation mechanism of the alloy at 300 °C compared to room

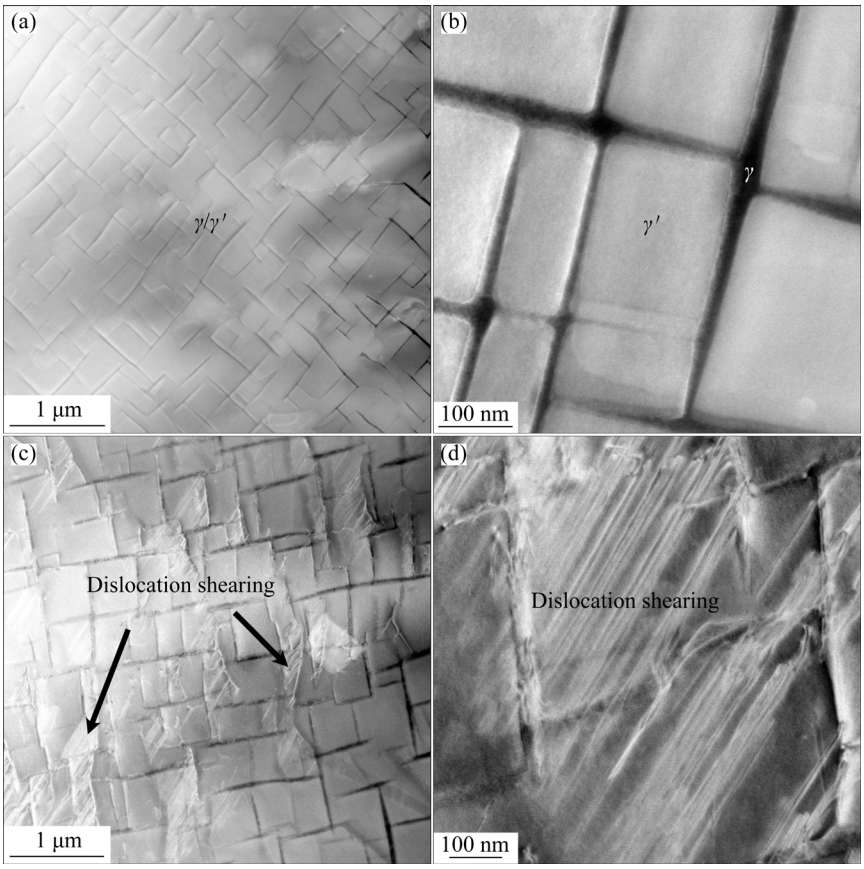

Fig. 5 STEM HAADF images along [001] zone axis for Co−30Ni−10Al−3V−6Ti−2Ta superalloy (a, b) undeformed and (c, d) deformed to ~0.2% at room temperature

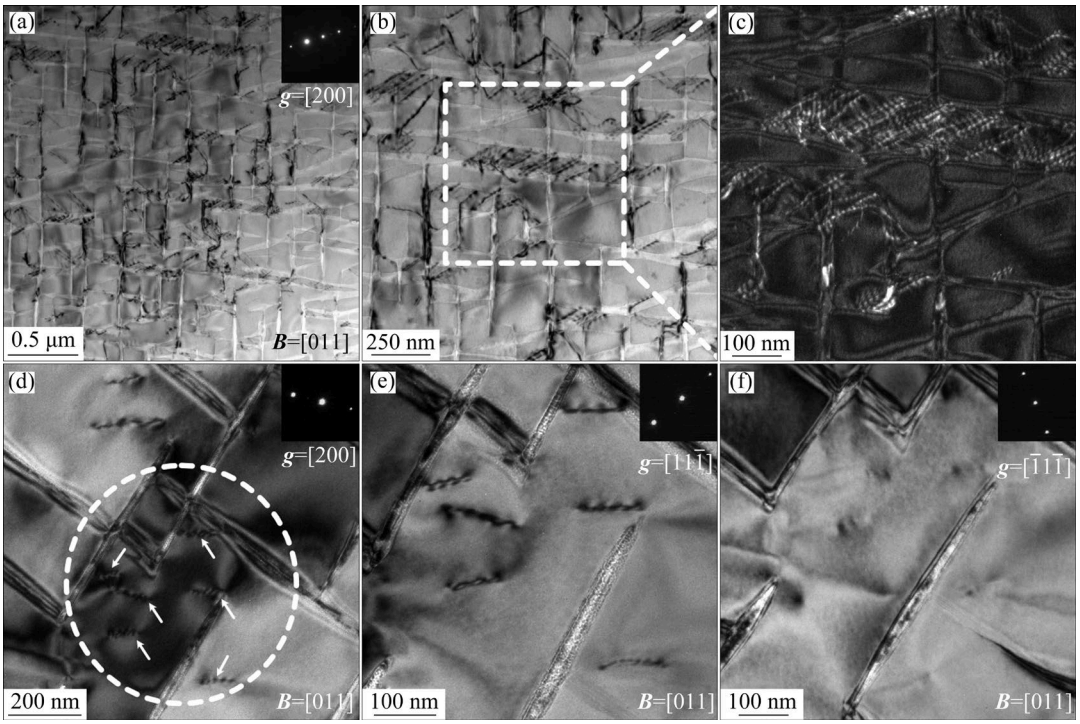

Fig. 6 (a, b) TEM bright field images and (c) TEM weak beam dark field image taken along [011] zone axis using superlattice 200 reflection; (d−f) TEM bright field images taken along another [011] zone axis using superlattice [200], $[11\bar{1}]$, and $[\bar{1}1\bar{1}]$ reflection for Co−30Ni−10Al−3V−6Ti−2Ta superalloy deformed to ~0.2% at 300 °C, respectively

temperature lies in the fact that the type of shear dislocation shifts from extended dislocation to superlattice dislocation pairs.

Figure 7(a) shows STEM HAADF image along [001] zone axis for Co−30Ni−10Al−3V−6Ti−2Ta superalloy deformed to ~0.2% at 650 °C. It shows superlattice dislocations shearing γ' phase, which is consistent with the shearing mechanism of dislocations at 300 °C. Figures 7(b, c) depict TEM brightfield images of superlattice dislocation pairs taken along [001] and [122] zone axis. It is indicated that the extended dislocation dissociates into superlattice dislocation pairs after shearing the γ' phase. Among them, α and β respectively denote two superlattice dislocation pairs, where $\alpha 1$ represents a leading partial dislocation and $\alpha 2$ a trailing dislocation, while $\beta 1$ and $\beta 2$ exhibit similar characteristics. It is important to note that $\alpha 1$ and $\alpha 2$ are two independent partial dislocations under the [122] zone axis, forming a superlattice dislocation pair known as APB-coupled. On the other hand, $\beta 1$ and $\beta 2$ demonstrate the invisibility of partial dislocation segments due to the sliding of APB-coupled superlattice dislocation pairs from (111) to (001), referred to as K−W locks. Additionally, features resembling K−W locks are also observed in Fig. 6(f), consistent with the research findings of WANG et al [53] and ZHANG et al [54].

Figures 7(d−f) show the TEM images of the superlattice dislocation pairs under different superlattice reflections ($\boldsymbol{g}$=[020], $\boldsymbol{g}$=[$\bar{2}$20] and $\boldsymbol{g}$=[200]). Table 1 summarizes the intensity of superlattice dislocation pairs under different superlattice reflections according to Figs. 7(d−f). The dislocations d_{1-3} and d_5 exhibit consistent visibility (V, I, V) under different superlattice reflections ($\boldsymbol{g}$=[020], $\boldsymbol{g}$=[220] and $\boldsymbol{g}$=[200]), which suggests that their Burger's vector is [110]. The superlattice dislocation pair, d_4 and d_6, are visible under different diffraction reflections, indicating their Burger's vector is $[\bar{1}10]$. It is worth noting that the Burger's vector for dislocation d_7 cannot be determined under three diffraction reflections. However, based on the Burger's vector of other dislocations, it can be inferred that the Burger's vector of d_7 should be $[10\bar{1}]$ or [101].

In this work, the dissociation form of ⟨110⟩ superlattice dislocations in the $L1_2$ structure on the {111} plane is as follows:

For superlattice dislocations $d_{1,3}$:

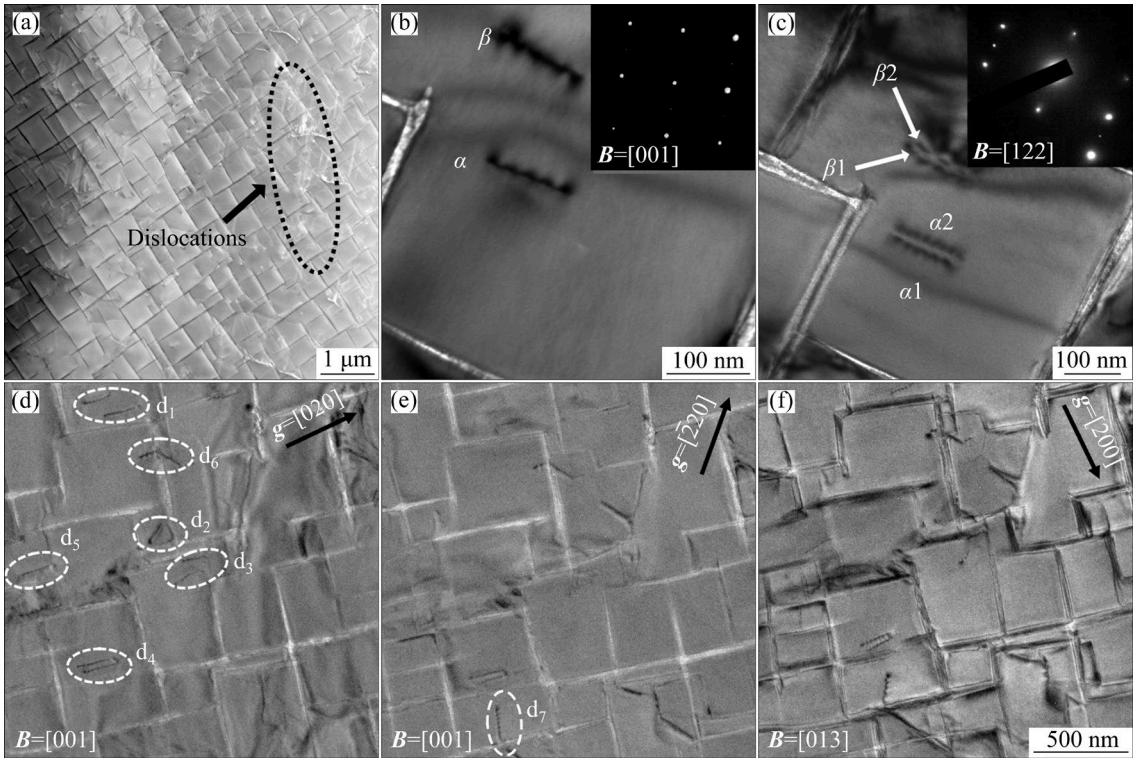

Fig. 7 STEM HAADF image along [001] zone axis (a) and TEM bright field images (b, c) taken along [001] and [122] zone axis, (d, e) taken along [001] using superlattice [020] and [$\bar{2}$20] reflection, and (f) taken along [013] using superlattice [200] reflection for Co−30Ni−10Al−3V−6Ti−2Ta superalloy deformed to ~0.2% at 650 °C

Table 1 Intensity of superlattice dislocation pairs under different superlattice reflections

Reflection,	Superlattice dislocation						
g	d_1	d_2	d_3	d_4	d_5	d_6	d_7
[020]	V	V	V	V	V	V	I
$[\bar{2}20]$	I	I	I	V	I	V	V
[200]	V	V	V	V	V	V	V
Burger's vector	[110]	[110]	[110]	$[\bar{1}10]$	[110]	$[\bar{1}10]$	$[10\bar{1}]$/[101]

V: Visible; I: Invisible

$$a[110]\rightarrow\frac{a}{2}[110]+\text{APB}+\frac{a}{2}[110] \quad (1)$$

Similarly, for superlattice dislocation d_4:

$$a[\bar{1}10]\rightarrow\frac{a}{2}[\bar{1}10]+\text{APB}+\frac{a}{2}[\bar{1}10] \quad (2)$$

Therefore, the deformation mechanism of the Co−30Ni−10Al−3V−6Ti−2Ta superalloy at 650 °C is partial dislocation shearing γ' phase, which involves the dissociation of extended dislocations into $a/2\langle 110\rangle$ superlattice dislocation pairs, and the shear form is represented by anti-phase boundaries (APB).

Figure 8 demonstrates TEM brightfield images taken along [001] zone axis using superlattice [220] reflection for the Co−30Ni−10Al−3V−6Ti−2Ta superalloy deformed to ~0.2% at 900 °C. It is found that (1) the dislocation accumulation around the γ' phase occurs (red arrow in Fig. 8(a)), (2) the number of superlattice dislocation pairs decreases (the white arrow in Fig. 8(b)), (3) the dislocation density in the γ phase increases (the red arrow in Fig. 8(b)), and (4) complex stacking faults (SFs) appear at the edge of the γ' phase (black arrow in Fig. 8(c)). Among them, the density of SFs differs from the research findings of Co−Ti based superalloy. For instance, in Co−12Ti and Co−12Ti−4Mo alloys, a significant presence of SFs was noted at 700 °C [55]. Similarly, in the Co−11Ti−15Cr alloy, a notable abundance of stacking faults was observed at 850 °C [19]. However, in this study, only a minimal quantity of SFs is observed at 900 °C, suggesting that the Co−30Ni−10Al−3V−6Ti−2Ta superalloy exhibits higher SF energy. Additionally, at 900 °C, a significant amount of dislocation shearing of the γ' phase is observed, accompanied by the formation of dislocation loops (Fig. 8(b)). Two factors can explain this phenomenon: (1) As the temperature increases,

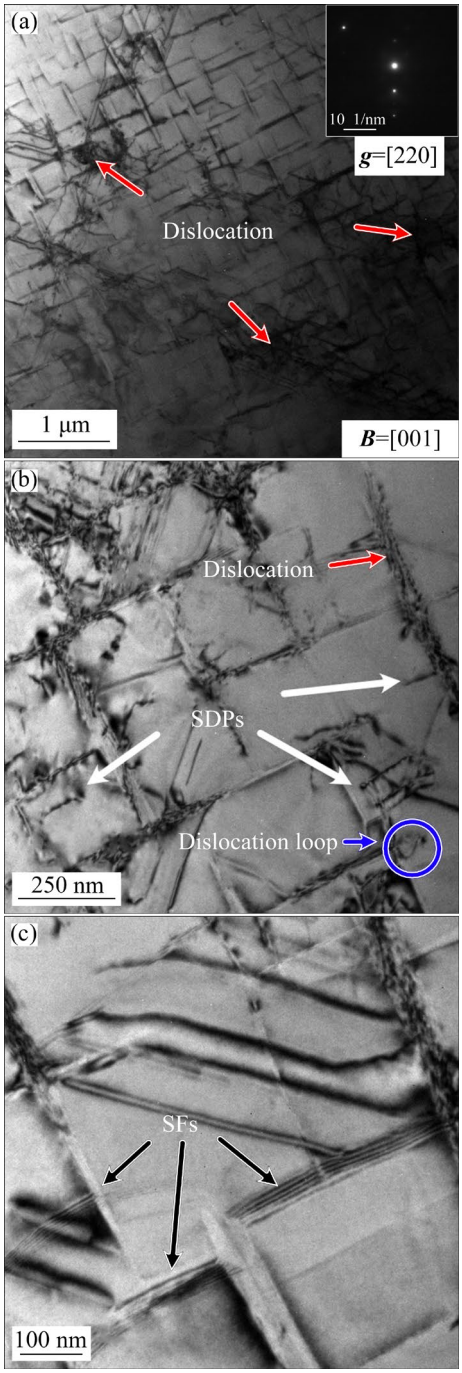

Fig. 8 TEM bright field images taken along [001] zone axis using superlattice [220] reflection for Co−30Ni−10Al−3V−6Ti−2Ta superalloy deformed to ~0.2% at 900 °C

the activation energy for dislocation movement decreases, making the dislocations move more easily and intensely at higher temperatures. Since the dislocation movement is a microscopic manifestation of the macroscopic deformation in the alloy, this explains why the alloy deforms more readily at high temperatures. (2) At high temperatures, $a/2[110]$ superpartial dislocations

decompose into *a*/3 or *a*/6 [112] partial dislocations, accompanied by the formation of stacking faults, which further weakens the strengthening effect of K−W Lock, leading to reduction in yield strength at 900 °C [52,56]. It should be noted that the formation of stacking faults does not necessarily imply a reduction in strength. The *a*/6⟨112⟩ Shockley partial dislocations can further decompose at high temperatures to form *a*/3⟨001⟩ immobile rod dislocations, known as Hirth Lock, or *a*/6⟨110⟩ immobile rod dislocations, known as L−C Lock [57,58]. Both of these deformation mechanisms can help maintain higher mechanical properties at high temperatures. However, since this study did not investigate the interactions among stacking faults, the sliding of stacking faults remains one of the main reasons for the degradation of performance of the alloy beyond 900 °C.

Based on these findings, the primary deformation mechanism of Co−30Ni−10Al−3V−6Ti−2Ta superalloy from room temperature to 900 °C is the shear of dislocations in γ' phase. It is noteworthy that the form of dislocation shear changes with different deformation temperatures. Specifically, at room temperature, the shearing form is the primary dislocation shear of the γ' phase. Between 300 and 650 °C, there is a transition to the shear of the γ' phase by APB-coupled superlattice dislocations, and beyond 900 °C, it gradually transforms into partial dislocation shear of the γ' phase by SFs. The transition in deformation mechanisms can be attributed to the differences in the formation mechanisms of APBs and SFs. The formation of APBs is an adiabatic process, independent of local atomic diffusion. When the external energy provided (i.e., temperature and deformation) exceeds the energy barrier of APBs, they are generated. In contrast, the formation of SFs is a result of atomic diffusion [59,60]. Under sufficient temperature and time, solute atom segregation tends to occur at the SF sites, leading to phase transformation of the $L1_2$ phase, thereby weakening the strengthening effect of the $L1_2$ phase. Therefore, the maintenance of yield stress between 300 and 650 °C is primarily caused by the strengthening effect of K-W locks. The reduction in YSA onset temperature is attributed to the high SF energy of the Co−30Ni−10Al−3V−6Ti−2Ta superalloy, which further supports previous studies [44,52]. Furthermore, the elevated γ' dissolution temperature is the key factor contributing to the higher abnormal yield stress observed in comparison to traditional Co−Ti based superalloy.

4 Conclusions

(1) The Co−30Ni−10Al−3V−6Ti−2Ta alloy demonstrates a high γ' dissolution temperature (1234 °C) and low density (8.15 g/cm³), with experimental data showing good agreement with CALPHAD predictions.

(2) Between 28 and 650 °C, the yield strength of the Co−30Ni−10Al−3V−6Ti−2Ta alloy increases, displaying distinct abnormal yield behavior.

(3) The onset of abnormal yield behavior at relatively low temperatures is attributed to the high stacking fault energy of the alloy, while the enhanced yield strength is primarily driven by the strengthening effect of K−W locks.

CRediT authorship contribution statement

Yu-peng ZHANG: Methodology, Validation, Formal analysis, Investigation, Data curation, Writing − Original draft; **Zhong-feng CHEN:** Resources, Supervision; **De-bin ZHENG:** Methodology, Formal analysis; **Cui-ping WANG:** Conceptualization, Resources, Supervision, Writing – Review & editing, Project administration, Funding acquisition; **Hao-jun ZHUO:** Methodology, Formal analysis; **Xiang YU**: Methodology, Formal analysis; **Yue-chao CHEN:** Resources, Supervision; **Shui-yuan YANG:** Writing − Review & editing, Supervision; **Yi-lu ZHAO:** Writing − Review & editing, Supervision, Funding acquisition; **Xing-jun LIU:** Conceptualization, Resources, Project administration, Funding acquisition.

Declaration of competing interest

The authors declare that they have no known competing financial interests or personal relationships that could have appeared to influence the work reported in this paper.

Data availability

The original contributions presented in the study are included in the article/Supplementary Materials. Further inquiries can be directed to the corresponding authors.

Acknowledgments

This study was supported by the National Natural Science Foundation of China (Nos. 51831007, 52101135),

the Shenzhen Science and Technology Program, China (No. SGDX20210823104002016), and the Guangdong Basic and Applied Basic Research Foundation, China (Nos. 2021B1515120071, JCYJ20220531095217039).

The authors would like to acknowledge Professor Guang RAN, Mr. Zhe-hui ZHOU (College of Energy, Xiamen University) for their help with TEM experiments. We would also like to thank Dr. Jayalakshmi SUBRAMANIAN and Dr. Arvind Singh RAMACHANDRA for their assistance in refining the article.

References

[1] REED R C. The superalloys: Fundamentals and applications [M]. Cambridge: Cambridge University Press, 2008.

[2] MEETHAM G W. The development of gas turbine materials [M]. London: Applied Science Publishers, 1981.

[3] DURAND-CHARRE M. The microstructure of superalloys [M]. Boca Raton: Routledge, 2017.

[4] WU Yu-ting, LI Chong, XIA Xing-chuan, LIANG Hong-yan, QI Qi-qi, LIU Yong-chang. Precipitate coarsening and its effects on the hot deformation behavior of the recently developed γ'-strengthened superalloys [J]. Journal of Materials Science & Technology, 2021, 67: 95−104.

[5] LI Shi-wei, LI Jing-long, SHI Jun-miao, PENG Yu, PENG Xuan, SUN Xian-jun, JIN Feng, XIONG Jiang-tao, ZHANG Fu-sheng. Microstructure and mechanical properties of transient liquid phase bonding DD5 single-crystal superalloy to CrCoNi-based medium-entropy alloy [J]. Journal of Materials Science & Technology, 2022, 96: 140−150.

[6] FAN Jiang-kun, YANG Hong-ci, ZHANG Pei-zhe, LI Jia-yu, JING Zhan-jie, CHEN Fu-long, LIU De-gui, TANG Bin, KOU Hong-chao, LI Jin-shan. Mechanism of high temperature oxidation of Inconel 625 superalloy with various solution and ageing heat treatment processes [J]. Transactions of Nonferrous Metals Society of China, 2024, 34(11): 3662−3676.

[7] WANG Kai-ming, LIU Wei, DU Dong, CHANG Bao-hua, LIU Guan, HU Yong-le, TONG Yong-gang, ZHANG Ming-jun, ZHANG Jian, JU Jiang. Microstructure and properties of K648 superalloy additively manufactured by extreme high-speed laser metal deposition [J]. Transactions of Nonferrous Metals Society of China, 2024, 34(7): 2192−2203.

[8] SIMS C T, STOLOFF N S, HAGEL W C. Superalloys II: High-temperature materials for aerospace and industrial power [M]. New York: Wiley, 1987.

[9] LI Zheng, ZHANG Zhen-lin, WU Ai-ping, ZHANG Ming-jun, KANG Ju, LIU Qu, ZHAO Yue, CHEN Jing-yang. Microstructure and mechanical properties of laser welded and post-weld heat-treated K439B superalloy [J]. Transactions of Nonferrous Metals Society of China, 2024, 34(3): 905−917.

[10] HE Yi-xuan, BU Fan, BIAN Zhang-chi, XIANG Ming-xiu, ZHOU Meng-meng, LIU Xu-dong, ZHU Lei, WANG Jun, LI Jin-shan. Evading strength−ductility trade-off of GH605 alloy using magnetic field-assisted undercooling treatment [J]. Transactions of Nonferrous Metals Society of China, 2024, 34(8): 2575−2588.

[11] SATO J, OMORI T, OIKAWA K, OHNUMA I, KAINUMA R, ISHIDA K. Cobalt-base high-temperature alloys [J]. Science, American Association for the Advancement of Science, 2006, 312(5770): 90−91.

[12] POLLOCK T M, DIBBERN J, TSUNEKANE M, ZHU J, SUZUKI A. New Co-based γ–γ' high-temperature alloys [J]. JOM, 2010, 62: 58−63.

[13] BOCCHINI P J, SUDBRACK C K, NOEBE R D, DUNAND D C, SEIDMAN D N. Effects of titanium substitutions for aluminum and tungsten in Co−10Ni−9Al−9W (at.%) superalloys [J]. Materials Science and Engineering A, 2017, 705: 122−132.

[14] MAKINENI S K, SAMANTA A, ROJHIRUNSAKOOL T, ALAM T, NITHIN B, SINGH A K, BANERJEE R, CHATTOPADHYAY K. A new class of high strength high temperature cobalt based γ–γ' Co−Mo−Al alloys stabilized with Ta addition [J]. Acta Materialia, 2015, 97: 29−40.

[15] YAN H Y, VORONTSOV V A, DYE D. Alloying effects in polycrystalline γ' strengthened Co−Al−W base alloys [J]. Intermetallics, 2014, 48: 44−53.

[16] BOCCHINI P J, LASS E A, MOON K W, WILLIAMS M E, CAMPBELL C E, KATTNER U R, DUNAND D C, SEIDMAN D N. Atom-probe tomographic study of γ/γ' interfaces and compositions in an aged Co−Al−W superalloy [J]. Scripta Materialia, 2013, 68: 563−566.

[17] LIU Xing-jun, WANG Yi-chun, XU Wei-wei, HAN Jia-jia, WANG Cui-ping. Effects of transition elements on the site preference, elastic properties and phase stability of L12 γ'-$Co_3(Al,W)$ from first-principles calculations [J]. Journal of Alloys and Compounds, 2020, 820: 153179.

[18] LASS E A, GRIST R D, WILLIAMS M E. Phase equilibria and microstructural evolution in ternary Co−Al−W between 750 and 1100 °C [J]. Journal of Phase Equilibria and Diffusion, 2016, 37(4): 387−401.

[19] BEZOLD A, VOLZ N, LENZ M, ZENK C H, SPIECKER E, MILLS M, GÖKEN M, NEUMEIER S. Yielding behavior of a single-crystalline γ'-strengthened Co−Ti−Cr superalloy [J]. Scripta Materialia, 2021, 200: 113928.

[20] LIU Xing-jun, PAN Yun-wei, CHEN Yue-chao, HAN Jia-jia, YANG Shui-yuan, RUAN Jing-jing, WANG Cui-ping, YANG Yuan-sheng, LI Ying-ju. Effects of Nb and W additions on the microstructures and mechanical properties of novel γ/γ' Co−V−Ti-based superalloys [J]. Metals, Multidisciplinary Digital Publishing Institute, 2018, 8(7): 563.

[21] PANDEY P, MAKINENI S K, SAMANTA A, SHARMA A, DAS S M, NITHIN B, SRIVASTAVA C, SINGH A K, RAABE D, GAULT B, CHATTOPADHYAY K. Elemental site occupancy in the L12 A3B ordered intermetallic phase in Co-based superalloys and its influence on the microstructure [J]. Acta Materialia, 2019, 163: 140−153.

[22] NITHIN B, SAMANTA A, MAKINENI S K, ALAM T, PANDEY P, SINGH A K, BANERJEE R, CHATTOPADHYAY K. Effect of Cr addition on γ–γ' cobalt-based Co−Mo−Al−Ta class of superalloys: A combined experimental and computational study [J]. Journal of Materials Science, 2017, 52(18): 11036−11047.

[23] CHEN Yue-chao, WANG Cui-ping, RUAN Jing-jing, YANG Shui-yuan, OMORI T, KAINUMA R, ISHIDA K, HAN Jia-jia, LU Yong, LIU Xing-jun. Development of low-density γ/γ' Co−Al−Ta-based superalloys with high solvus temperature [J]. Acta Materialia, 2020, 188: 652−664.

[24] GAO Shuang, SONG Zhen-feng, HE Bo, ZHOU Lan-zhang, HOU Jie-shan. Effect of Ta addition on solidification microstructure and element segregation of IN617B nickel-base superalloy [J]. Transactions of Nonferrous Metals Society of China, 2022, 32(2): 559−568.

[25] CHEN Yue-chao, WANG Cui-ping, RUAN Jing-jing, OMORI T, KAINUMA R, ISHIDA K, LIU Xing-jun. High-strength Co−Al−V-base superalloys strengthened by γ'-$Co_3(Al,V)$ with high solvus temperature [J]. Acta Materialia, 2019, 170: 62−74.

[26] ZHUANG Xiao-li, LU Song, LI Long-fei, FENG Qiang. Microstructures and properties of a novel γ'-strengthened multi-component CoNi-based wrought superalloy designed by CALPHAD method [J]. Materials Science and Engineering A, 2020, 780: 139219.

[27] MAKINENI S K, NITHIN B, CHATTOPADHYAY K. Synthesis of a new tungsten-free γ–γ' cobalt-based superalloy by tuning alloying additions [J]. Acta Materialia, 2015, 85: 85−94.

[28] ZENK C H, POVSTUGAR I, LI Rui, RINALDI F, NEUMEIER S, RAABE D, GÖKEN M. A novel type of Co−Ti−Cr-base γ/γ' superalloys with low mass density [J]. Acta Materialia, 2017, 135: 244−251.

[29] SINGH M P, MAKINENI S K, CHATTOPADHYAY K. Achieving lower mass density with high strength in Nb stabilised γ/γ' Co−Al−Mo−Nb base superalloy by the replacement of Mo with V [J]. Materials Science and Engineering A, 2020, 794: 139826.

[30] XU W W, HAN J J, WANG Z W, WANG C P, WEN Y H, LIUA X J, ZHU Z Z. Thermodynamic, structural and elastic properties of Co_3X (X=Ti, Ta, W, V, Al) compounds from first-principles calculations [J]. Intermetallics, 2013, 32: 303−311.

[31] XU Wei-wei, WANG Yi, WANG Cui-ping, LIU Xing-jun, LIU Zi-kui. Alloying effects of Ta on the mechanical properties of γ' $Co_3(Al,W)$: A first-principles study [J]. Scripta Materialia, 2015, 100: 5−8.

[32] WANG Cui-ping, YAN Li-hui, HAN Jia-jia, XU Wei-wei, DENG Bin, LIU Xing-jun. Effects of alloying elements on the structural, elastic and thermodynamic properties of Co_3Ta compounds from first-principles calculations [J]. Journal of Alloys and Compounds, 2017, 726: 490−497.

[33] XU W W, SHANG S L, WANG C P, GANG T Q, HUANG Y F, CHEN L J, LIU X J, LIU Z K. Accelerating exploitation of Co−Al-based superalloys from theoretical study [J]. Materials & Design, 2018, 142: 139−148.

[34] CHEN You-heng, WANG Cui-ping, ZHANG Chi, YANG Chen, HAN Jia-jia, LIU Xing-jun. Theoretical investigation of effects of transition elements on phase stabilities and elastic properties of the γ' phase in Co−V−Ta superalloys [J]. Frontiers in Materials, Frontiers, 2022, 9: 885608.

[35] PAN Shao-bin, YU Jin-xin, HAN Jia-jia, ZHANG Yan-qing, PENG Qing-hua, YANG Mu-jin, CHEN You-heng, HUANG Xiang, SHI Rong-pei, WANG Cui-ping, LIU Xing-jun. Customized development of promising Cu−Cr−Ni−Co−Si alloys enabled by integrated machine learning and characterization [J]. Acta Materialia, 2023, 243: 118484.

[36] RUAN Jing-jing, XU Wei-wei, YANG Tao, YU Jin-xin, YANG Shui-yuan, LUAN Jun-hua, OMORI T, WANG Cui-ping, KAINUMA R, ISHIDA K, LIU C T, LIU Xing-jun. Accelerated design of novel W-free high-strength Co-base superalloys with extremely wide γ/γ' region by machine learning and CALPHAD methods [J]. Acta Materialia, 2020, 186: 425−433.

[37] YU Jin-xin, WANG Cheng-lei, CHEN Yue-chao, WANG Cui-ping, LIU Xing-jun. Accelerated design of L12-strengthened Co-base superalloys based on machine learning of experimental data [J]. Materials & Design, 2020, 195: 108996.

[38] WANG Cui-ping, CHEN Xin, CHEN Yue-chao, YU Jin-xin, CAI Wen-su, CHEN Zhong-feng, YU Xiang, LI Ying-ju, YANG Yuan-sheng, LIU Xing-jun. Accelerated design of high γ' solvus temperature and yield strength cobalt-based superalloy based on machine learning and phase diagram [J]. Frontiers in Materials, 2022, 9: 882955.

[39] JIANG Heng-xing, YANG Shui-yuan, WANG Cui-ping, ZHANG Yan-qing, XU Xiao, CHEN Yue-chao, OMORI T, KAINUMA R, LIU Xing-jun. Martensitic transformation and shape memory effects in Co−V−Al alloys at high temperatures [J]. Journal of Alloys and Compounds, 2019, 786: 648−654.

[40] LIU Xing-jun, CHEN Zhong-feng, CHEN Yue-chao, YANG Shui-yuan, PAN Yun-wei, LU Yong, QU Sha-sha, LI Ying-ju, YANG Yuan-sheng, WANG Cui-ping. Multicomponent Co−Ti-based superalloy with high solvus temperature and low lattice misfit [J]. Materials Letters, 2021, 284: 128910.

[41] XINGJUN L I U, ZHENBANG W E I, YONG L U, JIAJIA H A N, RONGPEI S H I, CUIPING WANG. Progress on the diffusion kinetics of novel Co-based and Nb−Si-based superalloys [J]. Acta Metall Sin, 2023, 59(8): 969−985.

[42] LI Ling-ling, WANG Cui-ping, YANG Shui-yuan, HAN Jia-jia, LU Yong, ZHANG Jin-bin, LIU Xing-jun. Phase equilibria in Co−Ti−Re ternary system [J]. Rare Metals, 2023, 42(8): 2736−2746.

[43] WANG Cui-ping, CHEN You-heng, ZHUO Hao-jun, CAI Wen-su, CHEN Yue-chao, YU Xiang, YANG Shui-yuan, LI Ying-ju, YANG Yuan-sheng, LIU Xing-jun. Development of Co−Ni−Al−V−Ta−Cr-based superalloys with high-temperature strength and excellent oxidation resistance [J]. Journal of Materials Research and Technology, 2023, 27: 8143−8150.

[44] CHEN Zheng-hao, KISHIDA K, INUI H, HEILMAIER M, GLATZEL U, EGGELER G. Improving the intermediate- and high-temperature strength of L12-$Co_3(Al,W)$ by Ni and Ta additions [J]. Acta Materialia, 2022, 238: 118224.

[45] WANG Cui-ping, LE Jian-ping, CHEN Ke-ying, YANG Chen, YU Jin-xin, GUO Yi-hui, ZHUO Hao-jun, ZHANG Jin-bin, HAN Jia-jia, LIU Xing-jun. A novel Co−Ni−Ti−V-based superalloy exhibiting low density and high strength [J]. Materials Science and Engineering A, 2023, 885: 145633.

[46] WANG Cui-ping, ZHUO Hao-jun, ZHENG De-bin, YU Xiang, CHEN Xiao-dong, CHEN Yue-chao, CHEN Xin, ZHANG Jin-bin, HAN Jia-jia, LIU Xing-jun. Development of a low-density Co−Ni−Al−Ta−Cr superalloy with high mechanical performance and superior oxidation resistance [J]. Materials & Design, 2024, 238: 112673.

[47] LI Wen-da, LI Long-fei, ANTONOV S, LU F, FENG Q. Effects of Cr and Al/W ratio on the microstructural stability, oxidation property and γ' phase nano-hardness of multi-component Co−Ni-base superalloys [J]. Journal of Alloys and Compounds, 2020, 826: 154182.

[48] BALER N, PANDEY P, SINGH M P, MAKINENI S K,

CHATTOPADHYAY K. Effects of Ti and Cr Additions in a Co−Ni−Al−Mo−Nb-based superalloy [C]//TIN S, HARDY M, CLEWS J, et al. Superalloys 2020. The Minerals, Metals & Materials Series. Springer, Cham, 2020: 929−936.

[49] REYES TIRADO F L, TAYLOR S, DUNAND D C. Effect of Al, Ti and Cr additions on the γ−γ′ microstructure of W-free Co−Ta−V-based superalloys [J]. Acta Materialia, 2019, 172: 44−54.

[50] RUAN J J, LIU X J, YANG S Y, XU W W, OMORI T, YANG T, DENG B, JIANG H X, WANG C P, KAINUMA R, ISHIDA K. Novel Co−Ti−V-base superalloys reinforced by L12-ordered γ′ phase [J]. Intermetallics, 2018, 92: 126−132.

[51] PANDEY P, MUKHOPADHYAY S, SRIVASTAVA C, MAKINENI S K, CHATTOPADHYAY K. Development of new γ′-strengthened Co-based superalloys with low mass density, high solvus temperature and high temperature strength [J]. Materials Science and Engineering A, 2020, 790: 139578.

[52] FAN Zhong-ding, WANG Chen-chong, ZHANG Chi, YU Yun-he, CHEN Hao, YANG Zhi-gang. The temperature dependence of high-temperature strength and deformation mechanism in a single crystal CoNi-base superalloy [J]. Materials Science and Engineering A, 2018, 735: 114−120.

[53] WANG Tian-jian, ZHANG Hong, LIU Chun-hua, GONG Xiu-fang, PEI Yu-bing, ZOU Yu, LIU Yong-jie, WANG Qing-yuan. Effect of temperature on tensile behavior, fracture morphology and deformation mechanisms of Nickel-based single crystal CMSX-4 [J]. Journal of Alloys and Compounds, 2022, 912: 165175.

[54] ZHANG Hong, WANG Quan-yi, GONG Xiu-fang, WANG Tian-jian, ZHANG Wei, CHEN Ke, WANG Chong, LIU Yong-jie, WANG Qing-yuan. Dependence on temperature of compression behavior and deformation mechanisms of nickel-based single crystal CMSX-4 [J]. Journal of Alloys and Compounds, 2021, 866: 158878.

[55] IM H J, LEE S, CHOI W S, MAKINENI S K, RAABE D, KO W S, CHOI P P. Effects of Mo on the mechanical behavior of γ/γ′-strengthened Co−Ti-based alloys [J]. Acta Materialia, 2020, 197: 69−80.

[56] YANG Wen-chao, QU Peng-fei, LIU Chen, CAO Kai-li, QIN Jia-run, SU Hai-jun, ZHANG Jun, REN Cui-dong, LIU Lin. Temperature dependence of compressive behavior and deformation microstructure of a Ni-based single crystal superalloy with low stacking fault energy [J]. Transactions of Nonferrous Metals Society of China, 2023, 33(1): 157−167.

[57] HIRTH J P, LOTHE J. Theory of dislocations [M]. Malabar, FL, Krieger Pub Co, 1992.

[58] ARROYO ROJAS DASILVA Y, KOZAK R, ERNI R, ROSSELL M D. Structural defects in cubic semiconductors characterized by aberration-corrected scanning transmission electron microscopy [J]. Ultramicroscopy, 2017, 176: 11−22.

[59] TITUS M S, MOTTURA A, BABU VISWANATHAN G, SUZUKI A, MILLS M J, POLLOCK T M. High resolution energy dispersive spectroscopy mapping of planar defects in L12-containing Co-base superalloys [J]. Acta Materialia, 2015, 89: 423−437.

[60] MAKINENI S K, LENZ M, NEUMEIER S, SPIECKER E, RAABE D, GAULT B. Elemental segregation to antiphase boundaries in a crept CoNi-based single crystal superalloy [J]. Scripta Materialia, 2018, 157: 62−66.

基于 CALPHAD 方法设计的低密度 Co−Ni−Al−V−Ti−Ta 高温合金的独特屈服行为

张玉朋[1,2]，陈忠奉[1,2]，郑德斌[1,2]，王翠萍[1,2]，
卓淏鋆[1,2]，余 翔[1,2]，陈悦超[1,2]，杨水源[1,2]，赵怡潞[3]，刘兴军[3]

1. 厦门大学 材料学院 福建省高性能表界面工程重点实验室，厦门 361005；
2. 厦门大学 材料学院 厦门市高性能金属材料重点实验室，厦门 361005；
3. 哈尔滨工业大学(深圳) 材料科学与工程学院，深圳 518055

摘 要：低密度高温合金在中等温度范围(300~650 ℃)通常表现出较低的屈服强度。为了提高该温度范围内的屈服性能，采用 CALPHAD 方法设计了新的钴基高温合金。基于 γ′相溶解温度和相分数，设计并通过电弧熔炼和热处理合成了 Co−30Ni−10Al−3V−6Ti−2Ta 合金。通过差示扫描量热法、扫描电子显微镜、双束透射电子显微镜和压缩测试分别研究了合金的相变温度、微观结构演变和高温力学性能。结果表明，该合金具有低密度(8.15 g/cm^3)和高 γ′溶解温度(1234 ℃)，并表现出从室温至 650 ℃范围内的独特屈服强度保持特性。屈服强度异常现象(YSA)归因于较高的堆垛层错能和 Kear−Wilsdorf 锁强化机制的激活，这些因素提高了合金的高温稳定性。在 23~650 ℃温度范围内，该合金的屈服强度显著高于其他已报道的低密度钴基高温合金。

关键词：Co 基高温合金；计算相图；力学性能；亚结构演变；γ′相

(Edited by Bing YANG)